Altered Tissue 3′-Deoxy-3′-[^{18}F]Fluorothymidine Pharmacokinetics in Human Breast Cancer following Capecitabine Treatment Detected by Positron Emission Tomography

Laura M. Kenny,[1] Kaiyumars B. Contractor,[1] Justin Stebbing,[1] Adil Al-Nahhas,[2] Carlo Palmieri,[1] Sami Shousha,[3] R. Charles Coombes,[1] and Eric O. Aboagye[1]

Abstract

Purpose: We showed in preclinical models that thymidylate synthase (TS) inhibition leads to redistribution of the nucleoside transporter, ENT1, to the cell membrane and hence increases tissue uptake of [^{18}F]fluorothymidine (FLT). In this study, we assessed for the first time the altered pharmacokinetics of FLT in patients following administration of capecitabine, a drug whose mode of action has been reported to include TS inhibition.

Experimental Design: We analyzed 10 lesions from six patients with breast cancer by positron emission tomography before and after treatment with capecitabine. Although drug treatment did not alter tumor delivery pharmacokinetic variables (K1 and permeability product surface area) or blood flow, tumor FLT retention variables increased with drug treatment in all but one patient.

Results: The baseline average standardized uptake value at 60 minutes, rate constant for the net irreversible transfer of radiotracer from plasma to tumor (Ki), and unit impulse response function at 60 minutes were 11.11×10^{-5} m^2/mL, 4.38×10^{-2} mL plasma/min/mL tissue, and 4.93×10^{-2}/min, respectively. One hour after capecitabine administration, the standardized uptake value was 13.55×10^{-5} m^2/mL ($P = 0.004$), Ki 7.40×10^{-2} mL plasma/min/mL tissue ($P = 0.004$), and impulse response function was 7.40×10^{-2}/min ($P = 0.002$). FLT pharmacokinetics did not change in normal tissues, suggesting that the effect was largely restricted to tumors ($P = 0.55$).

Conclusions: We have identified FLT positron emission tomography retention parameters that could be used in future early clinical studies to measure the pharmacodynamics of TS inhibitors, as well as for identifying patients who are unlikely to benefit from TS inhibition.

(Clin Cancer Res 2009;15(21):6649–57)

Thymidylate synthase (EC 2.1.2.1.45; TS) continues to be an important target for cancer therapeutics due to its pivotal role in the *de novo* biosynthesis of DNA (1). The enzyme catalyses methylation of 2′-deoxyuridine-5′-monophosphate (dUMP) to 2′-deoxythymidine-5′-monophosphate and its inhibition results in the depletion of 2′-deoxythymidine-5′-monophosphate and of intracellular thymidine nucleotide pools. Clinical activity of TS inhibition in gastrointestinal cancers is seen with fluoropyrimidines such as 5-fluorouracil (5-FU) in combination with leucovorin, a reduced folate that stabilizes the binding of the 5-FU metabolite FdUMP to TS (2, 3). 5-FU inhibits TS, and thus, DNA synthesis (4). Capecitabine is an oral fluoropyrimidine prodrug, thought to be preferentially activated in tumor tissue, leading to improved intratumor drug concentrations and less systemic toxicity than 5-FU (3, 5). Selectivity of capecitabine is thought to be due to the higher expression of thymidine phosphorylase in tumor tissue compared with normal tissue (3). Capecitabine is metabolized to 5-FU through three metabolic steps. After absorption in the intestine, a carboxylesterase converts it to 5′-deoxyfluorocytidine. 5′-Deoxyfluorocytidine is then metabolized to deoxyfluorouridine by cytidine deaminase. The third and final step involves the conversion of deoxyfluorouridine to 5-FU by thymidine phosphorylase, which is expressed in solid tumors at levels 3 to 10 times that of surrounding normal tissues (4, 6). Intratumoral expression of TP has been shown to be a predictive marker of deoxyfluorouridine activity in breast cancer (7). Classic and nonclassic antifolate TS inhibitors including pemetrexed, raltitrexed, and

Authors' Affiliations: [1]Department of Oncology, Imperial College London, [2]Department of Nuclear Medicine, Imperial College Healthcare NHS Trust, and [3]Department of Histopathology, Charing Cross Hospital, Imperial College Healthcare NHS Trust, London, United Kingdom

Received 5/18/09; revised 7/9/09; accepted 7/23/09; published OnlineFirst 10/27/09.

Grant support: The United Kingdom Medical Research Council (U1200.005.00001.01) and Cancer Research UK (C37/A5610 and C2536/A10337).

The costs of publication of this article were defrayed in part by the payment of page charges. This article must therefore be hereby marked *advertisement* in accordance with 18 U.S.C. Section 1734 solely to indicate this fact.

Note: Supplementary data for this article are available at Clinical Cancer Research Online (http://clincancerres.aacrjournals.org/).

Requests for reprints: Eric O. Aboagye, Molecular Therapy and PET Oncology Research Group, Imperial College London, Faculty of Medicine, Hammersmith Hospital, Room 240 MRC Cyclotron Building, Du Cane Road, London W12 ONN, United Kingdom. Phone: 44-208-383-3759; Fax: 44-208-383-1783; E-mail: eric.aboagye@imperial.ac.uk.

doi:10.1158/1078-0432.CCR-09-1213

Translational Relevance

We previously showed in preclinical models that thymidylate synthase (TS) inhibition leads to the redistribution of nucleoside transporter ENT1 to the cell membrane, resulting in increased flux of nucleosides including [^{18}F]fluorothymidine. This property of cells has therefore been exploited to detect TS inhibition *in vivo*. In this article, we show for the first time in humans that tumor [^{18}F]fluorothymidine uptake kinetics, determined by positron emission tomography imaging, increases soon after treatment with a TS inhibitor, capecitabine. The finding has implications for the imaging of TS inhibition in humans and should be useful in the early clinical development of novel TS inhibitors to determine optimal dose and tissue selectivity. It may also be useful in selecting patients unlikely to benefit from TS-based therapies.

nolatrexed have also been developed for the treatment of various cancers (8).

Inherent and acquired resistance to TS inhibitors is a major problem. In addition to reduced drug transport, resistance can arise via enhanced thymidine salvage (8–11), i.e., cells overcome thymidine nucleotide pool depletion by importing extracellular thymidine from blood and phosphorylating it to produce 2′-deoxythymidine-5′-monophosphate, a reaction catalyzed mainly by the enzyme thymidine kinase 1 (TK1; cytoplasmic thymidine kinase; EC2.7.1.21). Furthermore, it is important to assess the pharmacodynamics of TS inhibitors in tumors during drug development and for patient management. Assessment of TS inhibition currently relies on the measurement of plasma deoxyuridine levels (2, 12, 13). This biochemical assay is the consequence of an increase in levels of TS substrate dUMP and its nucleoside 2′-deoxyuridine following TS inhibition. Plasma deoxyuridine levels, however, reflect global TS inhibition in both tumor and normal TS-responsive tissues and not tumor alone.

To detect tumor-specific TS inhibition, we have adapted a biochemical feature of cells—increased salvage kinetics following TS inhibition (see Fig. 1)—for the noninvasive measurement of TS inhibition in living subjects using positron emission tomography (PET). We have proposed that radiolabeled nucleosides including 2-[^{11}C]thymidine and 3′-deoxy-3′-[^{18}F]fluorothymidine (FLT) are suitable as radiotracers for imaging TS inhibition (14–17). FLT, because of its longer half-life ($T_{1/2}$ of ^{18}F is 109.8 minutes compared with 20.4 minutes for ^{11}C), is more suitable for clinical scanning than 2-[^{11}C]thymidine. We recently showed *in vitro* and in mouse models of

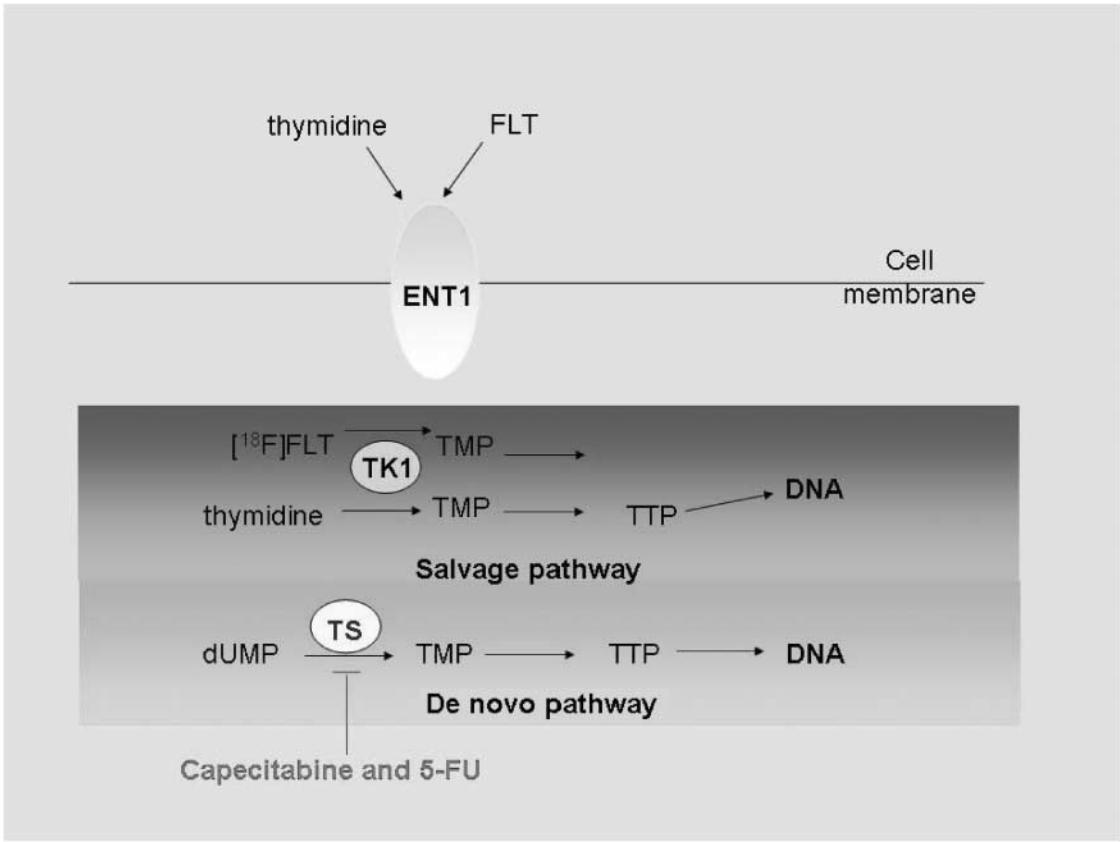

Fig. 1. The thymidine *de novo* and salvage pathways. The cell membrane transport of thymidine and FLT is facilitated by the equilibrative nucleoside transporter (ENT1). The action of FdUMP derived from capecitabine and 5-FU inhibit TS and thus the *de novo* pathway. Consequent to this, cells increase thymidine nucleotide pools via redistribution of ENT1 to the cell membrane (adapted from ref. 16).

Table 1. Patient demographics and imaging sites

Patient	Weight (kg)	Height (cm)	Imaging site	Sites of disease	Histology	Duration of treatment (d)	Response*	Duration of response (d)
1	57.6	159	Pelvis	Liver, bones, ovary	Grade 3 IDC ER-ve, PgR-ve, c-erbB2+++	85	PR	85
2	113.8	153	Upper thorax	Supraclavicular fossa	Grade 3 IDC ER+, PgR+ c-erbB2+++	336	PR	325
3	71.3	161	Breast, axilla	Bones, liver, lymph, breast	Grade 2 IDC ER+, PgR+, c-erbB2-ve	147	PR	147
4	83	157.5	Upper thorax and neck	Lymph nodes, liver	Grade 2 Lobular carcinoma ER-ve, PgR-ve, c-erb-ve	21	PD	N/a
5	64.6	168	Breast and contralateral axilla	Breast, lymph nodes	Grade 3 IDC ER+++/PgR+++ c-erbB2-ve	31	PD	N/a
6	79.2	155	Breast	Breast, bones	Grade 3 IDC ER+++, PgR-ve c-erbB2-ve	232	PR	252

Abbreviations: IDC, infiltrating ductal carcinoma; ER, estrogen receptor; PgR, progesterone receptor; PR, partial response; PD, progressive disease (21); N/a, not applicable.
*Response as defined using the Response Evaluation Criteria in Solid Tumors guidelines.

cancer that the increase in FLT uptake following TS inhibition was largely due to redistribution of nucleoside transporter ENT1 to the cell membrane within hours after drug administration; at these time points, TK1 expression was unaltered (16). Other mechanisms including enhanced TK1 expression may be involved in this unique biochemistry at late time points (in days; ref. 18). Given these proposed mechanisms of action, it is possible that FLT radiotracer kinetics could be dominated by delivery kinetics (because of enhanced transport) or retention kinetics (because phosphorylation by TK1 remains the rate-determining step in FLT uptake). The use of FLT-PET in a routine clinical setting (timing of a static FLT-PET scan) will require an objective understanding of FLT pharmacokinetics following drug administration: radiotracer delivery, retention, permeability product surface area (PS product) and the effect of tissue perfusion (blood flow). In this study, we have used capecitabine to investigate the effects of TS inhibition on FLT pharmacokinetics in patients with breast cancer.

Materials and Methods

Patients

Six patients with measurable locally advanced and metastatic breast cancer were studied. Ethical approval for the study was granted from the Hammersmith Hospital Research Ethics Committee. The study was done in accordance with the Declaration of Helsinki. Patients were recruited from the medical oncology clinics in Charing Cross Hospital, London (part of the Imperial NHS Healthcare Trust). The inclusion criteria were similar for previous FLT studies by our group (19, 20). Eligible patients had a breast tumor or regional lymph node lesion or metastasis measuring ≥2.0 cm, for which they were to receive treatment with capecitabine chemotherapy. All patients had American Joint Committee on Cancer stage III/IV breast cancer. Information sheets were given to all patients who were then given a minimum of 24 h to make a decision to participate in the study; informed consent was obtained for all patients. Patients were assessed for radiological and clinical response by the Response Evaluation Criteria in Solid Tumors guidelines during routine follow-up at medical oncology clinics as they continued their treatment with capecitabine (21). Details of the patients, sites of disease, duration of treatment, and treatment responses are shown in Table 1.

Study design and procedures

Radiochemical synthesis and scan procedure. All patients were scanned as outpatient procedures within Hammersmith Imanet, London on an ECAT HR+ 962 PET scanner (Siemens/CTI) that had a 15.5-cm axial field of view (transaxial, 58 cm). To ensure that changes in FLT pharmacokinetics were not due to variations in blood flow, we performed blood flow studies with [^{15}O]H_2O. A target dose of 600 MBq [^{15}O]H_2O was injected i.v. over 20 s followed by a 30-s flush with normal saline. Dynamic PET scanning was done for 10 min and 40 s in the following time frames: 30 s × 1, 20 s × 1, 5 s × 22, 10 s × 3, 30 s × 5, and 60 s × 5, from which the blood flow and volume of distribution were calculated. After a wait of 20 min to allow for decay of radioactivity (^{15}O half-life = 2.04 min), the FLT scan was done.

FLT was manufactured as described previously (22). The mean specific activity and mean radiochemical purity determined by high-performance liquid chromatography was 324.6 GBq/μmol and 99.7%, respectively. A target dose of 222 MBq of FLT was given as a bolus i.v. injection and dynamic PET scanning was done over 66 min and 30 s in the following frames: 30 s × 1, 10 s × 6, 15 s × 4, 30 s × 4, 120 s × 5, 180 s × 4, and 600 s × 4. Sinograms were Fourier-rebinned into two-dimensional slices and reconstructed (with correction for attenuation, scatter, and dead time) using filtered back-projection (ramp filter kernel full-width at half-maximum of 2.0 mm, 128 · 128 voxels of 2.62 · 2.62 mm^2, and slice thickness of 2.42 mm). The measured in-plane image resolution (transaxial) was 8.5 mm in full-width at half-maximum, and the axial image resolution was 5.0 mm. Before injection of the radiotracers, the tumor of interest was centered in the field of view, and a transmission scan was done using rotating ^{68}Ge sources for attenuation correction.

Patients were scanned on two separate occasions, the first before treatment, and the second within 1 h after the first oral dose of capecitabine, which was timed to coincide with the patients' scheduled

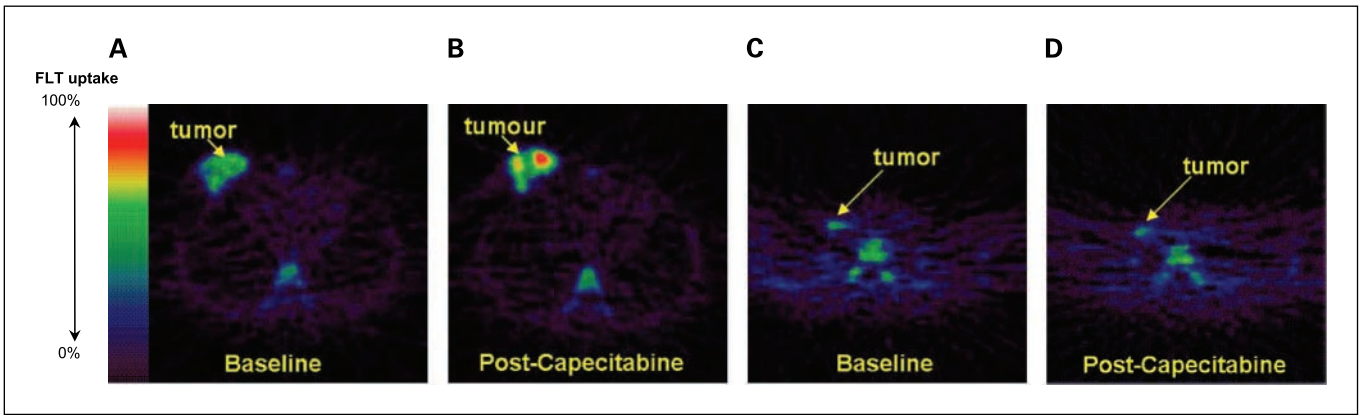

Fig. 2. Representative baseline and postcapecitabine FLT-PET images. Baseline (*A*) and posttreatment (*B*) images of a primary breast tumor (patient 6) that showed an increase in FLT uptake postcapecitabine. Baseline (*C*) and posttreatment (*D*) images in a patient with a cervical node (patient 4), which showed minimal change in FLT uptake.

treatment at 2 to 10 d after the baseline scan. The 1-h time point was selected to coincide with predicted maximum tumor drug levels as reported by Budman (23). In the Budman study, peak serum levels of capecitabine were seen at 1 to 2 h after ingestion. By performing FLT-PET scans between 1 and 2 h after dosing, we hoped to capture the peak plasma (and thus tissue) capecitabine and capecitabine metabolite levels. Because capecitabine is an oral drug, its targeting to tumors is dependent on the nutritional characteristics of the patient. To reduce variability, patients were advised to take capecitabine according to the instructions of the manufacturer, i.e., within 30 min of taking a meal. The weight and age of the patients studied (Table 1) do not seem likely to explain the alteration in FLT uptake. Capecitabine was administered to patients orally as 1,250 mg/m^2 divided into two doses for 14 d of a 21-d cycle (24).

Blood sampling and data analysis. To enable the assessment of FLT kinetics and blood flow, arterial blood was sampled via a radial artery cannula for measurement of radioactivity concentration simultaneously with the PET scan. For the [^{15}O]H_2O scan, blood sampling was done continuously throughout the scan at a rate of 5 mL/min following tracer injection until 1 min after the scan had been completed. For the FLT scan, continuous blood sampling was done for the first 10 min. In addition, discrete samples were taken at 2.5, 5, 10, 20, 30, 45, and 60 min (the first three samples were used for cross-calibration). Radioactivity in blood and plasma was measured as previously described (20). Furthermore, to permit the analysis of FLT kinetics, the proportions of FLT and FLT-glucuronide were assessed as previously described (20).

Definition of the region-of-interest was done by manually tracing the outline of the whole tumor or outer part of the tumor (in which an obvious necrotic core was identified) and normal tissues on multiple slices. Because the definition of tumor outlines was difficult on [^{15}O]H_2O images, regions-of-interest were first defined on FLT scans and the same outlines were applied to the [^{15}O]H_2O data sets. Image analysis was carried out using analysis software (Analyze Version 7; Biomedical Imaging Resource) as previously reported (20) to obtain time-activity curves.

Analysis of blood flow and FLT kinetics. Blood flow (F) and volume of distribution (V_d; the fraction of tissue volume into which [^{15}O]H_2O diffuses) were calculated using a modification of the one-tissue compartment model developed previously by Kety (25, 26) as shown in Eq. A below:

$$C_T(t) = F \times [C_a(t) \otimes \exp(-F/V_d \times t)] \qquad (A)$$

where $C_T(t)$ is the radioactivity concentration in tissue at time t, $C_a(t)$ is the radioactivity concentration in arterial blood at time t, F is regional blood flow (per mL of perfused tissue), V_d is the volume of distribution for water, which is defined as the ratio of the water concentration in tissue to that in blood at equilibrium, and $\otimes$ denotes the convolution operator. One of the limitations of the water flow model is that it assumes equivalent flow throughout the tumor—which may be inappropriate for larger lesions, especially those with areas of necrosis. For that reason, in this study, lesions larger than 5 cm were subdivided into separate tumor areas, and necrotic areas were not sampled.

Mathematical modeling and measurement of semiquantitative parameters for FLT was done as previously described (20). The following parameters were obtained: average standardized uptake value at 60 min (SUV_{60}), area under the time-activity curve (AUC), rate constant for the net irreversible uptake of FLT from plasma to tumor using the modified Patlak approach (Ki), and the unit impulse response function at 60 min (IRF_{60}) determined by spectral analysis (20, 27). K1, the rate constant describing delivery of FLT from plasma to tumor, was obtained by a two-tissue compartmental analysis (28). Furthermore, the permeability product surface area (PS) of FLT, a measure that reflects transport/extraction of the FLT into tumor from plasma, was calculated from the K1 value for FLT and F (obtained from analysis of [^{15}O]H_2O data) as follows:

$$PS = -F \times \ln.(1-K\ 1/F) \qquad (B)$$

Changes in the imaging pharmacokinetic variables above were compared with clinical response assessed after three cycles of capecitabine by conventional anatomic imaging (21).

Statistics. We defined objective increases in FLT uptake variables (Ki, SUV_{60}, IRF_{60}, and AUC) by comparison of the changes to the reference range of spontaneous fluctuations determined in a previous test-retest repeatability study (ref. 19; i.e., an increase in imaging variable of >95% confidence interval for variability). Furthermore, Wilcoxon-matched pairs test was used to determine if there was a statistically significant difference in tumor and normal tissues, and for all other parameters for which repeatability data were unavailable. Statistical analyses were done using GraphPad Prism version 4.

Results

No adverse events occurred in the study. The activity of injected FLT ranged between 147 and 234 MBq, and that of [^{15}O]H_2O was 566 and 777 MBq. Suitable PET images were obtained for the six patients. Clinical response was assessed in all patients. None of the patients had a complete response. Four patients had a partial clinical response and two patients died of progressive disease. The duration of treatment and response is shown in Table 1.

FLT imaging variables are altered in tumors but not normal tissues following capecitabine. The pharmacokinetics of FLT in 10 breast tumor regions were assessed by FLT-PET and [^{15}O]H_2O-PET. The lesion with the largest change in FLT-PET SUV_{60} was a primary breast tumor that showed a 50% increase in SUV_{60} (see Fig. 2). The smallest change was seen in a cervical node that showed a 1.35% decrease in uptake. With the exception of this cervical lesion, all other regions (nine regions from five patients) showed an increase in uptake measured by SUV_{60} at 1 hour postcapecitabine. The changes in SUV_{60}, AUC, IRF_{60}, and Ki are shown in Fig. 3, Table 2, and Supplementary Table S1.

When baseline and posttreatment tumor pharmacokinetic parameters were compared using the Wilcoxon matched pairs test, the increase in uptake was most significant for IRF_{60} (P = 0.002), followed by Ki and SUV_{60} (P = 0.0039), and lastly by AUC (P = 0.0098). Using SUV_{60} and AUC as imaging variables, a plot of the reference range of spontaneous fluctuations (19) identified four regions as having shown significant TS inhibition by imaging, i.e., changes in the imaging variable were above the upper solid line depicting ≥95% confidence for detecting a change (Fig. 4). These included an ovarian metastasis, a breast tumor, and two lesions in distinct regions from patient 6 who had a large breast tumor. All four lesions had a partial clinical response. Ki and IRF_{60} were significant for all but two lesions (i.e., for eight lesions in total). The significant changes matched those obtained by SUV_{60}. The two lesions that showed

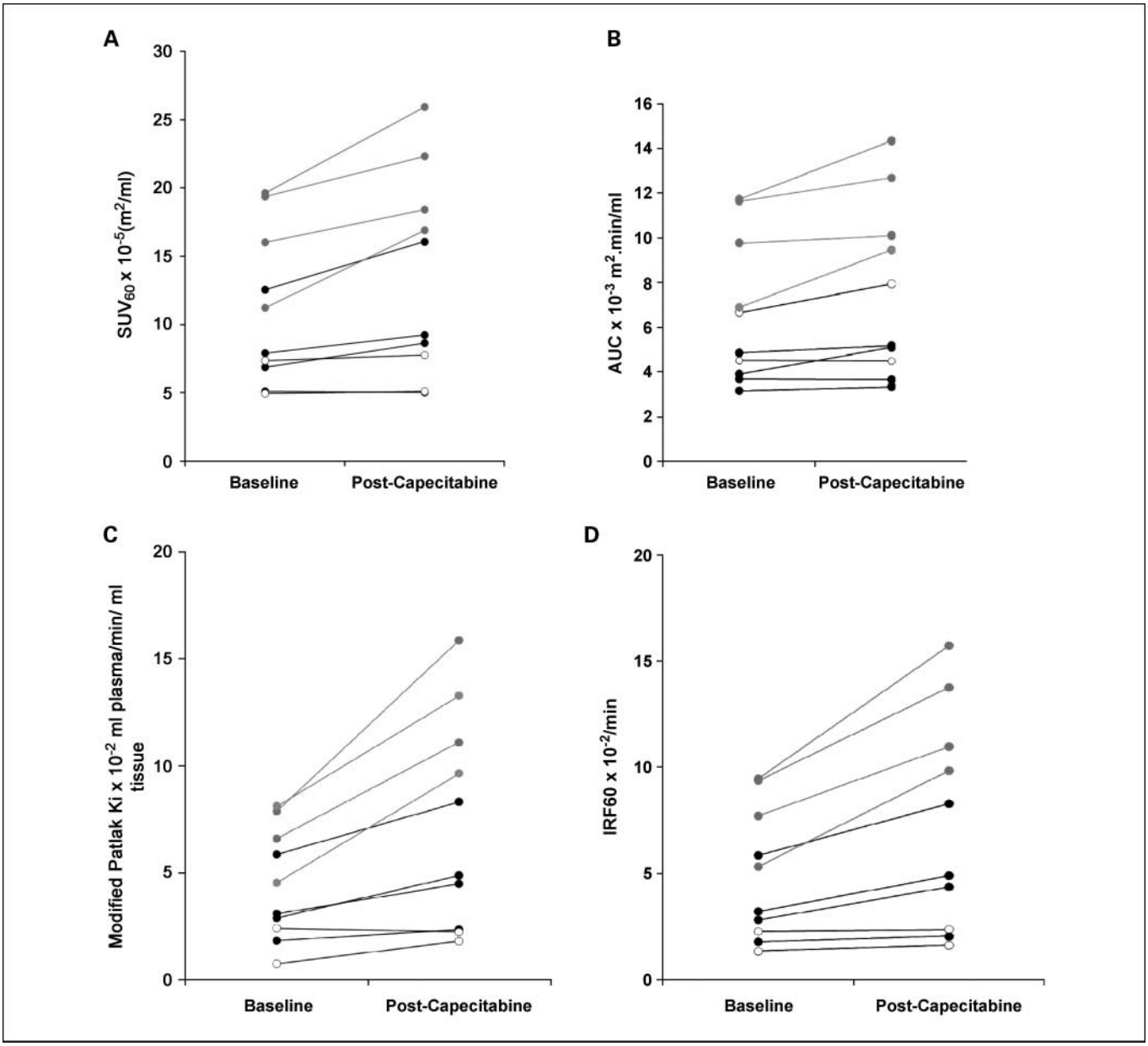

Fig. 3. FLT pharmacokinetic parameters precapecitabine and postcapecitabine: *A,* SUV_{60}; *B,* AUC; *C,* Ki; and *D,* IRF_{60}. Absolute values for each of the parameters are shown at baseline and postcapecitabine. White circles, the two lesions from patient 4 (breast and axilla); gray symbols and lines, the four lesions from patient 6.

Table 2. SUV_{60} values in tumor and normal tissue precapecitabine and postcapecitabine

Patient	Region	Baseline	Post-capecitabine
1	**Tumor**	**12.546**	**16.073**
1	Bowel	6.640	4.340
	Muscle	3.281	2.980
	Bone	13.832	17.992
2	**Tumor**	**7.909**	**9.252**
2	Lung	1.623	1.569
	Muscle	2.180	2.247
	Bone	10.694	8.195
3	**Tumor**	**6.867**	**8.644**
3	Bone	17.310	15.315
	Breast	1.001	1.720
	Muscle	1.389	0.572
4	**Tumor**	**5.108**	**5.039**
4	Lung	1.608	2.186
	Muscle	2.040	3.067
	Bone	19.504	22.188
5	**Tumor**	**4.965**	**5.119**
5	**Axillary node**	**7.354**	**7.763**
5	Muscle	1.270	0.983
	Lung	0.968	0.508
	Bone	12.501	11.202
6	**Tumor a**	**16.020**	**18.424**
	Tumor b	**11.228**	**16.917**
	Tumor c	**19.631**	**25.922**
	Tumor d	**19.376**	**22.306**
6	Lung	0.841	0.781
	Spleen	6.735	5.202
	Muscle	2.306	2.221
	Bone	14.918	15.831

NOTE: Where SUV_{60} = average SUV value at 60 min postinjection of FLT × 10^{-5} m^2/mL.

no significant response for any parameter occurred in the two patients with progressive disease.

SUV_{60} analysis of 19 normal tissue regions from lung, muscle, bone, bowel, and breast visualized within the field of view showed that there was no significant difference (Wilcoxon) in the uptake of FLT after treatment with capecitabine ($P = 0.55$; Table 2).

Tumor blood flow, V_d, and PS product. Blood flow was assessed in 8 of 10 regions. The remainder could not be assessed; in one case, there was a delay in commencing continuous blood sampling with a resultant loss of counting of the H_2 [^{15}O] peak radioactivity, and in another case, the data could not be fitted to the blood flow model. The mean tumor blood flow (±SEM) was 0.55 ± 0.07 mL/min/mL and 0.76 ± 0.17 mL/min/mL before and after capecitabine treatment, respectively (Table 3). This change was not statistically significant ($P = 0.25$). V_d of [^{15}O]H_2O was similar between the two groups ($P = 0.16$) and the PS of FLT was also similar between the two groups ($P = 0.74$).

Discussion

We have shown for the first time that FLT uptake in patients is increased in tumors, but not in normal tissue, within 1 hour following treatment with capecitabine with implications for use of FLT-PET in imaging TS inhibition in patients. TS inhibitors are in use for various malignancies and drug resistance is a major problem (5, 29). Furthermore, novel TS inhibitors including BGC 945 (17), and to a lesser extent, capecitabine (5), are tumor specific, requiring the monitoring of drug pharmacodynamics at the tumor level. The work reported here is the first human FLT-PET imaging protocol adapted for the measurement of TS inhibition. This method exploits a unique biochemistry of cells—the redistribution of ENT1 from the cytoplasm to the cell membrane within minutes to hours after administration of a TS inhibitor—to measure the pharmacodynamics of TS inhibitors (16). The increase in membrane ENT1 levels enhances the transport of FLT into the cells and makes more FLT available for phosphorylation by TK1 leading to enhanced trapping within cells. We have further validated the technology in tumor xenograft models with nonselective and tumor-selective TS inhibitors (17). As a prelude to the use of technology for early phase clinical studies in humans, we investigated the altered pharmacokinetics of FLT-PET in tumors of breast cancer patients treated with capecitabine.

We show in this study that compared with baseline levels, the uptake of FLT in tumors increases at 1 hour following the first oral administration of capecitabine. The increase in uptake was found to be dependent on the parameter used and ranged between 3.4% and 84.5% relative to baseline values. Both blood flow variables (F and V_d) and FLT delivery variables, K1 and PS, were largely unchanged after capecitabine treatment. In contrast, FLT retention variables SUV_{60}, AUC, Ki, and IRF_{60} increased in some tumors after drug treatment. This suggests that, although the biochemical mechanism of enhanced uptake of FLT following TS inhibition may involve the redistribution of ENT1 to the membrane, it is the trapping of the FLT-phosphate consequent to TK1 enzymatic activity that is primarily responsible for the enhanced uptake. This assertion may also explain why the relative increase in tumor FLT uptake was higher for modeled variables, Ki and IRF60, than semiquantitative variables, SUV and AUC. For any given retention variable, the intensity of enhanced FLT uptake was also found to be different for tumors in different patients and for different tumor lesions within the same patients. Without correlative biopsy analysis of TS inhibition, we can only speculate that this was due to different levels of TS inhibition in the different tumors. This speculation is supported by our earlier preclinical studies in which analyses of tumor and plasma dUrd levels—surrogate measures of TS inhibition—and FLT uptake were assessed together (16).

This is one of the first studies that reports simultaneous blood flow variables and FLT kinetics in the same tumors. Of note, the tumor FLT retention variables were not flow dependent. The lack of flow dependence in FLT uptake has implications for the wider use of FLT in monitoring therapy. Assessment of kinetic parameters showed objectively that a late imaging time point (60 minutes) was suitable for FLT-PET imaging of capecitabine pharmacodynamics. The delivery parameters did not change with drug treatment, whereas the retention parameters did. This implies that studies aimed at using FLT-PET for imaging TS inhibition could use static imaging at 60 minutes. However, it is obvious from this study that a dynamic imaging approach with blood sampling, arterial in this case but possibly venous (20, 30), will provide improved sensitivity and may enable the detection of smaller pharmacodynamic

effects in clinical trials of novel TS inhibitors. As previously mentioned, the decision to carry out the PET imaging studies at 1 hour after administering oral capecitabine was based on the predicted optimal tumor levels of capecitabine (23). In the Budman study (23), peak serum levels of capecitabine were seen at 1 to 2 hours postingestion. By performing FLT-PET scans between 1 and 2 hours after dosing, we hoped to capture the peak plasma (and thus tissue) capecitabine and capecitabine metabolite levels. Because capecitabine is an oral drug, its targeting to tumors is dependent on the nutritional characteristics of the patient. To reduce variability, patients were advised to take capecitabine according to the instructions of the manufacturer, i.e., within 30 minutes of taking a meal. The weight and age of the patients studied (Table 1) do not seem likely to explain the alteration in FLT uptake.

This time point will differ for different TS inhibitors depending on mechanism of action, pharmacokinetics of the drug candidate, and intensity and duration of TS inhibition. These parameters have to be assessed in preclinical studies before implementation in early human trials. A limitation of our feasibility study was that we were unable to fully assess the clinical value of the imaging technology (and relationship with deoxyuridine levels). However, FLT uptake did not change in the two types of proliferating normal tissues assessed—bowel and bone marrow—suggesting that the altered capecitabine pharmacodynamics was largely restricted to the tumor tissue. The sensitivity of using plasma deoxyuridine levels as a marker of capecitabine-induced TS inhibition may therefore be questionable; this could explain why deoxyuridine levels were not predictive of clinical outcome in patients with colorectal cancer. Furthermore, Ford and colleagues (12) have suggested that the relationship between TS inhibition and deoxyuridine levels are not linear, and that plasma deoxyuridine levels are thought to reflect duration rather than degree of TS inhibition. This, together with the fact that the salvage pathway contributes to a small proportion of the thymidine nucleotide pool compared with the *de novo* pathway, means that the two assays do not measure the same aspect of cellular pharmacology. Previous studies in mice have shown that TS-dependent FLT uptake increases in a dose-dependent fashion, supporting the use of FLT-PET to measure tumor TS inhibition for both tumor-selective and nonselective TS inhibitors (16, 17).

Although this article describes a feasibility study in six patients, the relationship between FLT-PET and subsequent clinical outcome is interesting. Future studies in a larger cohort of patients could establish the clinical value of FLT-PET for imaging TS inhibition in patients and explore the inclusion of a second posttreatment scan performed after the chronic dosing phase of TS inhibitor, to determine if clinical response is also predicted by a subsequent decrease in FLT uptake/retention.

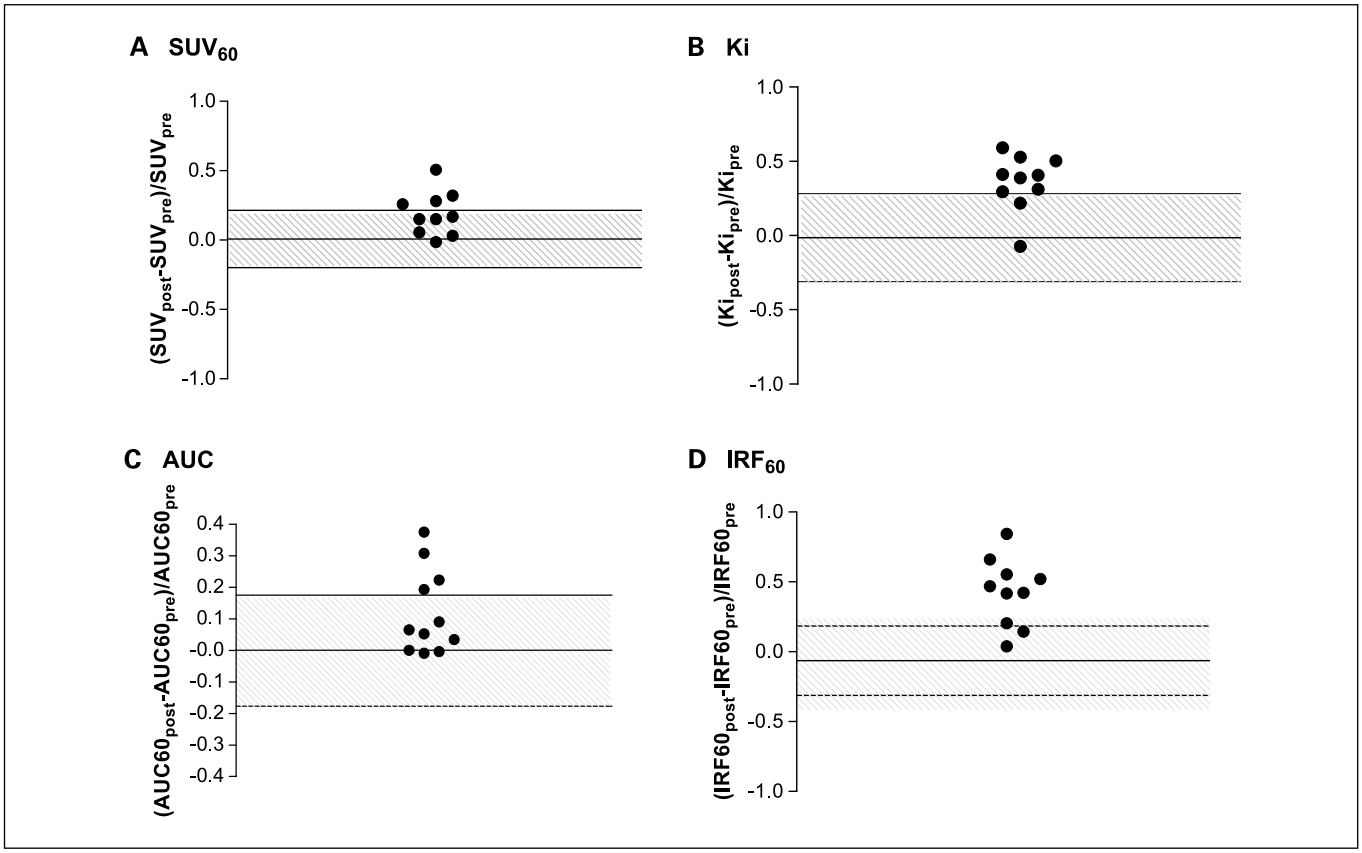

Fig. 4. Significance plots for FLT-PET pharmacokinetic parameters, SUV_{60} (*A*), AUC (*C*), Ki (modified Patlak) (*B*), and IRF_{60} (*D*). The significance was determined from our previous study of FLT-PET repeatability (19). Values above the upper dotted line represent a significant increase, those in the shaded gray area show changes that cannot be distinguished from noise variations, and those below the lower dotted line represent a significant decrease in FLT uptake.

Table 3. Comparison of tumor radiotracer delivery variables precapecitabine and postcapecitabine determined by $[^{15}O]H_2O$-PET only

Region	F_{pre}	F_{post}	AUC_{pre}	AUC_{post}	$V_{d\ pre}$	$V_{d\ post}$	$K1_{pre}$	$K1_{post}$	PS_{pre}	PS_{post}
Tumor	0.52	*0.52*	1.27	*1.50*	0.93	*0.97*	0.16	*0.16*	186.1	*186.9*
Tumor	0.98	*0.34*	0.60	*0.83*	0.32	*0.47*	0.07	*0.15*	71.0	*202.7*
Tumor	0.31	*0.26*	0.93	*0.90*	0.54	*0.60*	0.10	*0.37*	124.2	*370.3*
Tumor	0.25	*0.14*	0.83	*0.63*	0.57	*0.59*	0.09	*0.08*	114.4	*112.5*
Axilla	*	*	1.15	*1.07*	0.64	*0.57*	0.42	*0.06*	638.4	*56.1*
Tumor a	0.50	*0.71*	1.25	*1.07*	0.76	*0.71*	0.23	*0.19*	*299.9*	*227.2*
Tumor b	0.44	*1.46*	0.82	*1.12*	0.46	*0.65*	0.14	*0.18*	*168.3*	*190.5*
Tumor c	0.58	*0.95*	1.05	1.27	0.63	*0.80*	0.30	*0.27*	427.4	*316.8*
Tumor d	0.61	*0.90*	1.25	1.18	0.75	*0.74*	0.24	*0.29*	309.5	*352.1*

NOTE: Blood flow (F), area under the $[^{15}O]H_2O$ time vs radioactivity curve (AUC), and volume of distribution (V_d). FLT-PET only (FLT delivery K1), and a combination of $[^{15}O]H_2O$ and FLT-PET (permeability PS area).
Columns in italics represent postcapecitabine values, the rest are precapecitabine values: blood flow, F (mL/min/mL tissue); $[^{15}O]H_2O$, AUC ($\times 10^{-3}$ m^2 min/mL); $[^{15}O]H_2O$, V_d (mL blood/mL tissue); K1 for FLT from compartmental analysis (mL/min/mL); PS product (mL/min/m).
*Values not included due to a poor fit of the model.

In conclusion, we have shown that the pharmacokinetics of FLT-PET is altered within 1 hour after treatment of breast cancer patients with capecitabine. We have identified retention parameters that could be used in future studies to measure the pharmacodynamics of TS inhibition. FLT-PET could play an important role in the assessment of novel TS inhibitors in early clinical evaluation, as well as for identifying patients who are resistant or unlikely to benefit from TS inhibition.

Disclosure of Potential Conflicts of Interest

No potential conflicts of interest were disclosed.

Acknowledgments

We thank the patients who participated in the research, our research nurse, Sian Thomas, and the radiographers and staff of Hammersmith Imanet who assisted with the scanning.

References

1. Wilson PM, Fazzone W, LaBonte MJ, Deng J, Neamati N, Ladner RD. Novel opportunities for thymidylate metabolism as a therapeutic target. Mol Cancer Ther 2008;7:3029–37.
2. Peters GJ, van der Wilt CL, van Groeningen CJ, Smid K, Meijer S, Pinedo HM. Thymidylate synthase inhibition after administration of fluorouracil with or without leucovorin in colon cancer patients: implications for treatment with fluorouracil. J Clin Oncol 1994;12:2035–42.
3. Meyerhardt JA, Mayer RJ. Systemic therapy for colorectal cancer. N Engl J Med 2005;352:476–87.
4. Curtin NJ, Harris AL, Aherne GW. Mechanism of cell death following thymidylate synthase inhibition: 2′-deoxyuridine-5′-triphosphate accumulation, DNA damage, and growth inhibition following exposure to CB3717 and dipyridamole. Cancer Res 1991;51:2346–52.
5. Walko CM, Lindley C. Capecitabine: a review. Clin Ther 2005;27:23–44.
6. Yarden Y, Baselga J, Miles D. Molecular approach to breast cancer treatment. Semin Oncol 2004;31:6–13.
7. Tominaga T, Toi M, Ohashi Y, Abe O. Prognostic and predictive value of thymidine phosphorylase activity in early-stage breast cancer patients. Clin Breast Cancer 2002;3:55–64.
8. Jackman AL, Theti DS, Gibbs DD. Antifolates targeted specifically to the folate receptor. Adv Drug Deliv Rev 2004;56:1111–25.
9. Jansen G, Schornagel JH, Westerhof GR, Rijksen G, Newell DR, Jackman AL. Multiple membrane transport systems for the uptake of folate-based thymidylate synthase inhibitors. Cancer Res 1990;50:7544–8.
10. Smith PG, Marshman E, Calvert AH, Newell DR, Curtin NJ. Prevention of thymidine and hypoxanthine rescue from MTA (LY231514) growth inhibition by dipyridamole in human lung cancer cell lines. Semin Oncol 1999;26:63–7.
11. Jones TR, Calvert AH, Jackman AL, Brown SJ, Jones M, Harrap KR. A potent antitumour quinazoline inhibitor of thymidylate synthetase: synthesis, biological properties and therapeutic results in mice. Eur J Cancer 1981;17:11–9.
12. Ford HE, Mitchell F, Cunningham D, et al. Patterns of elevation of plasma 2′-deoxyuridine, a surrogate marker of thymidylate synthase (TS) inhibition, after administration of two different schedules of 5-fluorouracil and the specific TS inhibitors raltitrexed (Tomudex) and ZD9331. Clin Cancer Res 2002;8:103–9.
13. Rafi I, Boddy AV, Calvete JA, et al. Preclinical and phase I clinical studies with the nonclassical antifolate thymidylate synthase inhibitor nolatrexed dihydrochloride given by prolonged administration in patients with solid tumors. J Clin Oncol 1998;16:1131–41.
14. Wells P, Aboagye E, Gunn RN, et al. 2-[11C] thymidine positron emission tomography as an indicator of thymidylate synthase inhibition in patients treated with AG337. J Natl Cancer Inst 2003;95:675–82.
15. Yau K, Price P, Pillai RG, Aboagye E. Elevation of radiolabelled thymidine uptake in RIF-1 fibrosarcoma and HT29 colon adenocarcinoma cells after treatment with thymidylate synthase inhibitors. Eur J Nucl Med Mol Imaging 2006;33:981–7.
16. Perumal M, Pillai RG, Barthel H, et al. Redistribution of nucleoside transporters to the cell membrane provides a novel approach for imaging thymidylate synthase inhibition by positron emission tomography. Cancer Res 2006;66:8558–64.
17. Pillai RG, Forster M, Perumal M, et al. Imaging pharmacodynamics of the α-folate receptor-targeted thymidylate synthase inhibitor BGC 945. Cancer Res 2008;68:3827–34.
18. Direcks WG, Berndsen SC, Proost N, et al. [18F]FDG and [18F]FLT uptake in human breast cancer cells in relation to the effects of chemotherapy: an *in vitro* study. Br J Cancer 2008;99:481–7.
19. Kenny L, Coombes RC, Vigushin DM, Al-Nahhas A, Shousha S, Aboagye EO. Imaging early changes in proliferation at 1 week post chemotherapy: a pilot study in breast cancer patients with 3′-deoxy-3′-[(18)F]fluorothymidine positron emission tomography. Eur J Nucl Med Mol Imaging 2007;34:1339–47.
20. Kenny LM, Vigushin DM, Al-Nahhas A, et al. Quantification of cellular proliferation in tumor and normal tissues of patients with breast cancer by [18F]fluorothymidine-positron emission tomography imaging: evaluation of analytical methods. Cancer Res 2005;65:10104–12.
21. Therasse P, Arbuck SG, Eisenhauer EA, et al. New guidelines to evaluate the response to treatment in solid tumors. European Organization for Research and Treatment of Cancer, National Cancer Institute of the United States, National Cancer Institute of Canada. J Natl Cancer Inst 2000;92:205–16.

22. Cleij MC, Brady F, Ell PJ, Pike VW, Luthra SK. An improved synthesis of 3′-deoxy-3′[18F] fluorothymdiine ([18F]FLT) and the fate of the precursor, 2,3′-anydro-5′-O-(4,4′-dimethoxytrityl)-thymidine. J Labelled Comp Radiopharm 2001; 44:S871–3.
23. Budman DR. Capecitabine. Invest New Drugs 2000;18:355–63.
24. Ershler WB. Capecitabine monotherapy: safe and effective treatment for metastatic breast cancer. Oncologist 2006;11:325–35.
25. Kety S. The theory and applications of exchange of inert gas at the lungs and tissues. Pharmacol Res 1951;3:1–41.
26. Anderson HL, Yap JT, Miller MP, Robbins A, Jones T, Price PM. Assessment of pharmacodynamic vascular response in a phase I trial of combretastatin A4 phosphate. J Clin Oncol 2003;21:2823–30.
27. Cunningham VJ, Jones T. Spectral analysis of dynamic PET studies. J Cereb Blood Flow Metab 1993;13:15–23.
28. Aboagye EO, Price PM. Use of positron emission tomography in anticancer drug development. Invest New Drugs 2003;21: 169–81.
29. Longley DB, Harkin DP, Johnston PG. 5-Fluorouracil: mechanisms of action and clinical strategies. Nat Rev Cancer 2003;3:330–8.
30. Shields AF, Briston DA, Chandupatla S, et al. A simplified analysis of [18F]3′-deoxy-3′-fluorothymidine metabolism and retention. Eur J Nucl Med Mol Imaging 2005;32:1269–75.